Class. Quantum Grav. **13** (1996) A67–A78. Printed in the UK

Electrostatic accelerometers for the equivalence principle test in space

P Touboul†, M Rodrigues, E Willemenot and A Bernard

Office National d'Etudes et de Recherches Aerospatiales, BP 72, 92322 Chatillon Cedex, France

Abstract. The concept of the three-axis electrostatic accelerometers based on the full electrostatic suspension of one unique proof mass is very suitable for space applications requiring very high resolution of acceleration measurement or drag-free control of satellite. This concept has been tested in orbit with the accelerometer CACTUS from ONERA in the late seventies and recently with the accelerometer ASTRE on board Columbia shuttle in June 1996. The accelerometer outputs are derived from the measurement of the electrostatic forces, necessary to maintain the mass motionless at the centre of the accelerometer cage. The relative test-mass position and attitude are servo-controlled from measurements of capacitive sensors exhibiting resolutions of better than 10^{-10} mHz$^{-1/2}$ depending on the geometrical configuration.

The test of the weak equivalence principle can be performed in orbit on board a drag-free satellite with two concentric electrostatic accelerometers including two cylindrical test masses made of different materials. The measured common acceleration is controlled to null along the three directions by the drag compensation system of the satellite. The differential acceleration is detected at the orbital frequency (or around the satellite spin frequency) along the common revolution axis with an expected resolution of 10^{-14} ms^{-2} Hz$^{-1/2}$. The differential disturbing acceleration induced by magnetic, electric and thermal disturbances must be limited to this value thanks to the 4 K environment of the sensor-head. The present definition of such an instrument is presented and the expected performances are detailed.

PACS number: 0480C

1. Overview

The objective of several space missions under study by the agencies NASA, ESA and CNES is to improve the resolution of the test of universality of free fall to 10^{-17} [1–3]. The cryogenic instrument, accommodated on board a drag-free satellite, is composed of very sensitive accelerometers each one including two concentric test masses made of different materials.

The in-orbit motions of the two test masses, maintained as free as possible, are carefully compared in order to estimate any equivalence principle (EP) violation signal. For that purpose magnetic superconducting accelerometers were first proposed by P Worden: the two test masses are magnetically suspended with superconducting coils and the differential motion of the test masses, coupled only by very weak 'magnetic springs', is measured using SQUIDs [4].

Another way to configure the experiment is to constrain the relative motion of the two test masses and any EP violation will appear through the forces (or accelerations) that will be necessary to keep the two test masses motionless with respect to each other.

† E-mail address: touboul@onera.fr

0264-9381/96/SA0067+12$19.50

This paper presents the configuration, presently envisaged and developed by the authors at ONERA, for this type of differential accelerometer specifically optimized for an in-orbit test of the equivalence principle. Two cylindrical test masses are electrostatically suspended along their axis of revolution. This axis will be the instrument's sensitive axis. The motion of each test mass along this axis is measured by linear capacitive sensors and is servo-controlled using electrostatic actuators. The voltages applied on the electrodes for this control will be the accelerometer outputs. The difference of the measured acceleration in the direction of the Earth (considered as the source of the gravitational attraction in this test) will be representative of any violation signal to be detected.

The main advantages of servo-controlled electrostatic accelerometers are the possibilities offered by the optimization of the configuration with respect to:

- relaxation of the required sensitivity of the position sensors (1 nm $Hz^{-1/2}$ is sufficient for an EP test to 1×10^{-17})
- reducing the effects of the parasitic electrical forces (due to contact potential differences, patch effects or to the test-mass charge) which may be a limitation if important motion occurs
- increasing the simplicity and reliability of flight operations and calibration; in particular, the switch-on mode of the instrument and the satellite attitude and drag compensation control
- ground tests and calibrations can be done at room temperature allowing, in particular, partial tests in micro-gravity in a drop tower or in a parabolic aircraft flight.

Furthermore, this differential accelerometer, called SAGE (space accelerometer for gravitation experiment), will comprise the sensor-head mechanics, that can operate at room or cryogenic temperature, and the functional electronics unit operating at room temperature. This accelerometer can also be applied to less ambitious missions (in terms of scientific return, cost and schedule) with a room-temperature instrument.

2. Accelerometer specifications and general configuration

2.1. SAGE general configuration

The SAGE instrument is composed of two concentric electrostatic accelerometers, each sensor head including a test mass and operating at liquid helium temperature (see figure 1). The cage of the accelerometer is made of fused silica and the necessary electrodes for the electrostatic suspensions are defined by gold coatings. The materials of the test masses have been selected according to their theoretical atomic properties [5] but also taking into account their physical characteristics, such as purity, homogeneity, machining ability, dimensional stability, magnetic susceptibility and electrical conductivity. With four differential accelerometers the following pairs of materials are proposed (for the 'internal'/'external' mass): Pt/Be, Pt/Si, Pt/Ti and Ti/Be.

Both accelerometers (in one SAGE instrument) will operate independently even if the main characteristics will have to be matched. The acceleration of each test mass will be measured along the three directions. The difference of the measured accelerations along the SAGE sensitive axis will be performed outside the electronic loops necessary for the operation of the suspension of each test mass. The configuration is optimized to enhance the resolution of this difference measurement.

The accelerometers are accommodated on board a drag-free satellite, in a circular orbit higher than 400 km, stabilized in an inertial frame or in a frame rotating about the normal

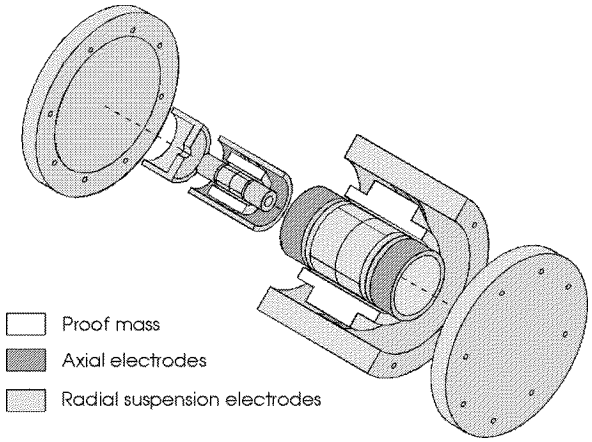

Figure 1. Space accelerometer for gravitation experiment: general configuration.

to the orbit (z axis) at a very low frequency f_r (a few times the orbital frequency f_0, i.e. 1.7×10^{-4} Hz). Their sensitive axes are in the orbital plane, two along x and two along y, for instance, and the Earth's gravitational attraction is projected in a sine wave leading to the EP violation signal detection at a well known frequency f_{EP} ($f_{EP} = f_r + f_0$) and phase.

2.2. Differential acceleration specifications

The EP test can be performed at a level better than 10^{-17} by achieving a differential acceleration sensitivity of 3×10^{-17} m s^{-2} at an altitude of 500 km. Thus, with an integrating period of the signal of about 20 orbits, corresponding to 10^5 s, the required resolution in the vicinity of the frequency f_{EP}, is 10^{-14} m s^{-2} Hz$^{-1/2}$ along the sensitive axis.

Parasitic accelerations in the differential mode induced by the test-mass environment (gravitational, magnetic, thermal and particularly electrical), must be limited to the same spectral density of 10^{-14} m s^{-2} Hz$^{-1/2}$ and to the expected resolution of 3×10^{-17} m s^{-2} at the frequency f_{EP}.

The test masses must be well centred to reduce the effects of the Earth's gravity gradient even though the major disturbance component will be at $2(f_0 + f_r)$. Frequency filtering of the signal reduces this disturbance by a factor of 100, in which case an off-centring of $< 1.5 \times 10^{-3}$ μm is required.

Such a centring cannot be achieved through machining accuracy. In fact, centring with an accuracy of only 15 μm can be guaranteed after the launch vibrations and the instrument is switched on. In-flight a specific electrical setting will reduce this off-centring to < 0.15 μm, and any residual gravity-gradient signal can be cancelled out in the data processing.

A more detailed analysis, performed by considering the gradient harmonics up to degree of order 5, has shown that these requirements remain sufficient if the test-mass moments of inertia are identical and the eccentricity of the orbit is 10^{-3} [6].

2.3. Common-mode acceleration specifications

As shown in the next paragraph, a rejection ratio of better than 10^{-4} is expected against accelerations applied in the common mode of the two accelerometers. This rejection is obtained from matching the accelerometer scale factors (to 10^{-4}) and by the alignments of the sensitive axes (to 10^{-4} rad).

In this case the common-mode acceleration must be lower than 10^{-10} m s^{-2} Hz$^{-1/2}$ in the three directions and at frequencies around f_{EP}. This is, in particular, a requirement on the performance of the drag compensation system of the satellite that will activate the helium thrusters to nullify the mean output of the accelerometers.

The Earth gravity gradient along the normal to the orbit may generate a disturbing signal applied in common mode when SAGE is at a distance larger than 15 μm from the orbital plane. Then, when the pointing of the satellite is inertial, the EP test can only be performed with the one SAGE instrument used to cancel out the applied common acceleration through the satellite propulsion control; the three other SAGE can be located along the z axis with an accuracy of several μm but at a necessary distance of several tens of centimetres.

2.4. Test-mass shapes

Another specification demanded for the design of SAGE concerns the test-mass shape. First, Worden has proposed cylindrical shapes [4]. Then, as shown in [7] by Lockerbie, test masses composed of an outer belted cylinder and a straight inner cylinder reduce the effects of any time-dependent self-gravity gradients of the satellite, especially helium tides. The concept of belted cylinders has been optimized for SAGE taking into account the constraints coming from the sensor head operation and production. In particular, flat areas have been added for control of the test-mass rotation about the sensitive axis and a minimum radial distance of 8 mm has been imposed between the two test masses in order to ease the production and integration of the silica accelerometer cages. We also relax the constraint of having the inner mass equal to the outer one.

The parameters to be optimized which describe the test-mass shapes are presented in figure 2. A mass M at a distance R from the centre of the two test masses creates a common acceleration $a \approx GM/R^2$, and a differential acceleration Δa that can be confused with an EP violation signal when the disturbing mass is rotating around SAGE at the EP frequency (worst case).

Thus $\Delta a/a$ must be minimized. It can be expressed as $\Delta a/a = (GM/R^2)(\sum_{p=1}^{\infty} c_{2p}/R^{2p})$, where c_{2p} depends on the test-mass geometries and on the two spherical coordinate angles that describe the position of M. Unlike in references [4] and [7], the two masses do not need to be equal in SAGE. It allows the same design of the silica cage to be kept for all four differential accelerometers. This has the benefit of simplicity and allows correlation data analysis. The optimization of the shapes can start from belted cylinder geometries meeting the conditions:

- c_2, c_4, c_6 null
- spherical inertia moments

and verifying:

- $r_3 - r_2 \geqslant 8.000$ mm for the feasibility of the electrode cylinders
- $r_4 - r_3 \geqslant 3.000$ mm for the test-mass geometry accuracy and stability
- test mass $\geqslant 30$ g for the accelerometer resolution.

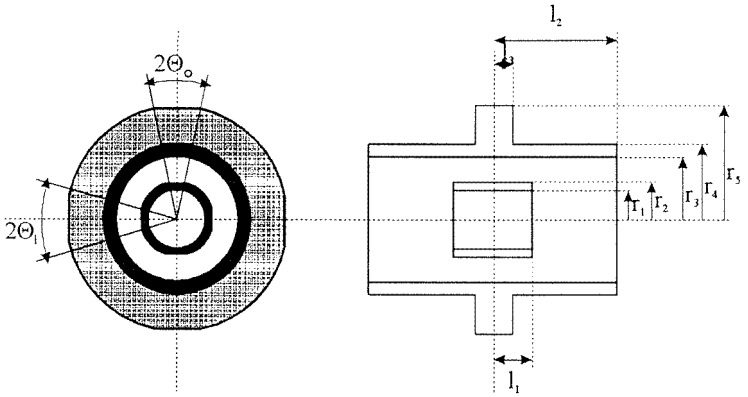

Figure 2. Test-mass shapes.

The three last relations are dictated by technological requirements from the mechanical sensor design and integration.

It must be realized that the performance obtained numerically with the optimization software when considering a mass M located on the axis of revolution, is extremely sensitive to the *a priori* frozen dimensions of the test masses. In particular, $(r_3 - r_2)$ (see figure 2) is the most sensitive parameter. This is the radial distance between the two test masses that includes the two accelerometer cages and two necessary gaps: $(r_3 - r_2)$ is kept as small as tolerable by the mechanical design.

We have also shown that the ratio $\Delta a/a$ is very sensitive to the absolute machining accuracy even if the test-mass geometry is optimized. For 1 μm defects of accuracy, the sensitivity is roughly 10 ppm at $R = 20$ cm, 4 ppm at $R = 25$ cm and 1 ppm at $R = 50$ cm.

After the first optimization process leading to the belted cylinders, flat areas are added with sufficient dimensions for the control of the test-mass spin. If the shapes are not re-optimized this leads to a sensitivity $\Delta a/a$ of several hundreds of parts per million. Hence $\Delta a/a$ must be minimized again using the parameters r_5, l_3 and l_2. The ratio $\Delta a/a$ is directly minimized without optimizing successively the coefficients of its development. The range of R corresponds to the dimensions of the He tank [8]. Selected parameters of the test-mass shapes are the following:

Table 1. Parameters of the test-mass shapes.

$r_1 = 8.000$ mm	$r_3 = 21.000$ mm	
$r_2 = 13.000$ mm	$r_4 = 24.000$ mm	
	$r_5 = 39.716$ mm	
$l_1 = 13.215$ mm	$l_2 = 60.000$ mm	$l_3 = 28.188$ mm
$\theta_i = 0.15$ rad	$\theta_0 = 0.15$ rad	

The sensitivity obtained, $\Delta a/a$, is plotted in figure 3 first as a function of R for θ and φ corresponding to the maximum value and then as a function of θ and φ for R minimum, i.e. 25 cm.

For test masses with flat areas, the ratio $\Delta a/a$ can be larger when the disturbing mass is away from the axis; it is maximum for $R = 25$ cm when θ and φ are varying but is always < 6 ppm. To obtain Δa lower than 3×10^{-17} m s^{-2}, the acceleration a must satisfy

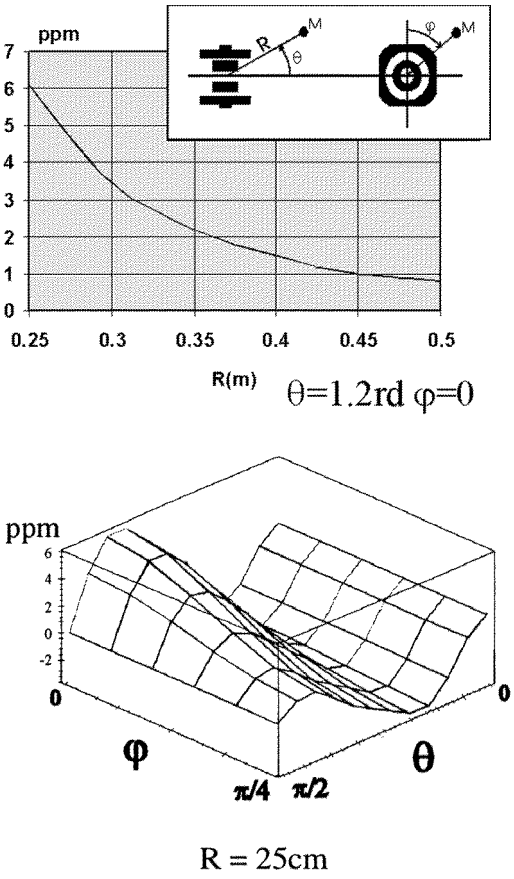

Figure 3. Sensitivity $\Delta a/a$ of the selected test-mass shapes.

$a < \Delta a/6 \times 10^{-6} \leftrightarrow a = GM/R^2 < 5 \times 10^{-12}$ m s^{-2}. At a distance R of 25 cm, the allowable disturbing mass of helium turning at the EP frequency around the instrument is then $M \approx 4.7$ g.

3. Accelerometer electrostatic configuration

The SAGE accelerometers are based on the same concept as the servo-controlled electrostatic accelerometers, GRADIO and ASTRE [9, 10] already developed in ONERA for space applications. A three-axis suspension is realized with six servo-control channels in order to stabilize (in position and attitude) the test mass at the centre of its cage. The applied electrostatic forces are measured to provide the three-axis accelerometer outputs.

As shown in figure 1, six pairs of electrodes, each associated with one channel, are used for both capacitive position sensing (six degrees of freedom) and electrostatic restoring force generation. At the ends of the test masses, the two cylindrical sensing electrodes allow measurement and control of the test-mass displacement along the axial direction while the eight quadrant electrodes, associated in pairs, allow measurement and control of the radial translations and rotations.

Along the sensitive axial direction, the configuration is such that the gradients of

capacitances between the electrodes and the mass are independent of the position of the test mass leading to a weak electrostatic negative stiffness induced by any test-mass potential. Furthermore, the electrode configuration ensures a very good linearity of the sensing of the axial position.

A correcting network (proportional–integral–derivative) determines the control voltages to be applied to the electrodes. Specific amplifiers deliver opposite and sufficiently high voltages for the generation of restoring forces according to the accelerometer full scale range. One unique AC detection voltage V_d (used for all capacitive sensors) and a DC bias voltage V_p are applied to the test mass through a very thin conducting wire.

Both electrodes attract the test mass with forces proportional to the capacitance gradients and to the square of the potential difference between them and the test mass: when the configuration is symmetric, the resultant force is proportional to the control voltage V and to the test-mass DC voltage V_p. V is measured and represents the cage kinematic acceleration minus the test-mass gravitational acceleration at frequencies where the test mass is motionless.

Figure 4 presents a simple block diagram of one control loop with the following notation:

- s: the Laplace derivative variable
- $\Gamma_c = s^2 x_c$: acceleration of the cage
- Γ_{el}: electrostatic applied acceleration (the instrument output through V)
- Γ_d: disturbing acceleration induced by the sensing device or any parasitic effect, such as thermal noise induced by the thin wire
- $x = x_{test\,mass} - x_c$: test-mass relative position with respect to the cage
- x_n: position sensor noise
- $\omega_p^2 = (2\pi f_p)^2$: parasitic stiffness induced by the test-mass potential (applied V_p, V_d and contact potential differences if any) and by the thin wire.

The test-mass motion is expressed by $s^2(x_c - x_{test\,mass}) = (\Gamma_c - (m_g/m_I)g) - (\Gamma_{el} + \Gamma_d) - \omega_p^2(x_c - x_{test\,mass})$ where g is the Earth's gravity field acting on the test mass. Γ_d can depend on s, x, because of dissipation.

Measurement of Γ_{el} represents the accelerometer output:

$$\Gamma_{el} = \frac{H(s)}{(s^2+\omega_p^2)+H(s)}\left(\Gamma_c - \frac{m_g}{m_I}g - \Gamma_d\right) + \frac{H(s)}{(s^2+\omega_p^2)+H(s)}(s^2+\omega_p^2)x_n$$

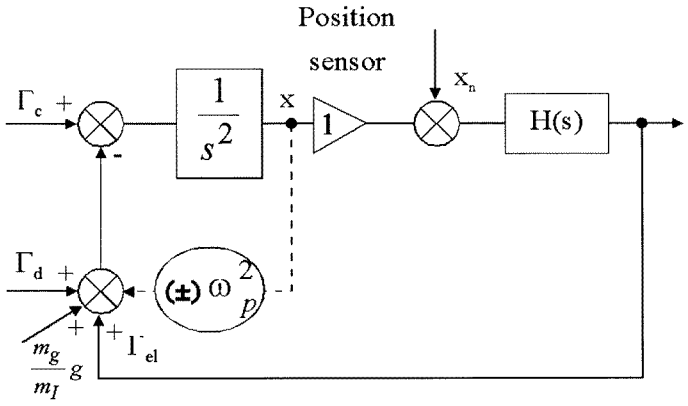

Figure 4. Simplified block diagram of one control loop.

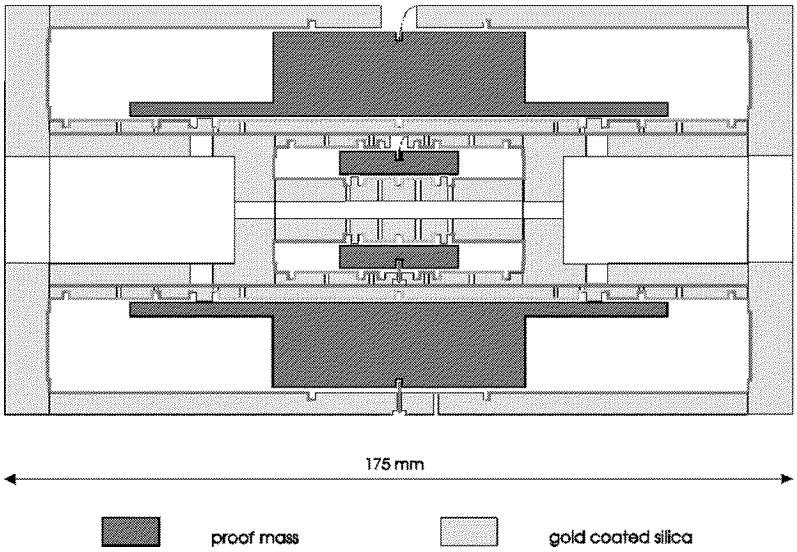

Figure 5. Design of SAGE laboratory model.

with $H(s)$ the transfer function of the loop that can be simplified as $H(s) \approx \omega_c^2 (1 + bs + c/s)$ where b and c provide the stability and the accuracy of the loop, respectively. The natural angular frequency of the closed loop ($\approx \omega_c$) can be selected around 1 rad s^{-1} corresponding to a bandwidth cut-off frequency f_c of about 0.2 Hz, much higher than the EP test frequency f_{EP} and the parasitic stiffness frequency, $H(s) \gg (s^2 + \omega_p^2)x_n$. The resolution of the measurement Γ_{el} is limited by parasitic accelerations and effects of the position sensor noise: $\Gamma_{el} \approx \Gamma_c - \Gamma_d + (s^2 + \omega_p^2)x_n - (m_g/m_I)g$. Then, the performance of the proposed concept relies on:

- the position sensor resolution
- stiffnesses induced by the wire (positive stiffness) and by the voltages V_p and V_d (negative stiffness): the electrostatic configuration and the capacitive sensors have been optimized in order to obtain f_p lower than f_{EP}
- the very weak level of test-mass disturbances Γ_d: the major sources are the test-mass damping (fluctuation dissipation theorem) induced by residual gas and the wire and electrostatic forces induced mainly by V_p and V_d when the configuration is not fully symmetric.

4. Design and evaluated performances

The design of the first laboratory model of the SAGE instrument is presented in figure 5. Manufacturing requirements have been taken over from the experience of ASTRE which used gold-coated ULE. The radial gaps between the test mass and its cage is 1 mm and the axial gap is about 15 mm: the axial electrostatic stiffness frequency has been evaluated with a finite element software model to be $< 10^{-5}$ Hz for 1 V applied to a 200 g test mass. Care has been taken to reduce the parasitic effects introduced if non-conducting areas face the test masses.

From the defined geometry, variations of all capacitances with respect to the test-mass motions have been evaluated leading to the sensitivity of the sensing and of the actuators.

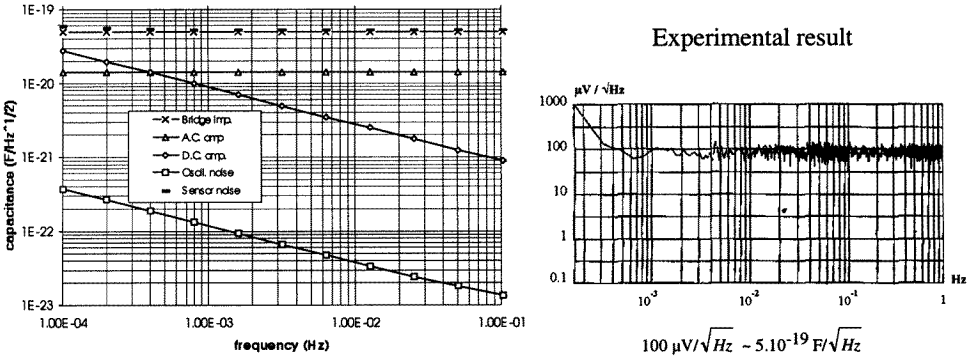

Figure 6. Capacitive sensor resolution.

Consequently, the detection voltage V_d has been selected as 5 V_{rms} and V_p as 1 V, limiting the induced negative electrostatic stiffness to an equivalent frequency $< 10^{-4}$ Hz. The resolution of the capacitive sensing is 6×10^{-8} pF $Hz^{-1/2}$ with a gain of 200 V pF^{-1}. Figure 6 presents evaluations of the different contributions to the detector noise and the resolution obtained with a circuit breadboard. In the capacitive sensor circuit, the detection voltage V_d, applied to the test mass is 'collected' through the electrode capacitance bridge constituted with two symmetric coils of a differential transformer. The sensor electronics is composed of an AC selective amplifier, a synchronous demodulation and a low-frequency amplifier that provides a DC voltage proportional to the difference of the two capacitances of the bridge. The electronics and the differential transformer are operated at room temperature. The circuit has been optimized to obtain white noise down to 10^{-4} Hz entirely due to the thermodynamic noise of the bridge loss resistance. This has been verified on a circuit breadboard down to 160 μHz, with a detection voltage V_d of 1 V (see figure 6).

With the selected geometry, the capacitive resolution corresponds to 3.8×10^{-11} m $Hz^{-1/2}$ for the inner mass axial position and 2.5×10^{-11} m $Hz^{-1/2}$ for the outer mass presenting larger electrodes.

The performance of both accelerometers constituting the SAGE instrument with a Pt and Ti test mass have been evaluated considering the four major noise sources: (i) the capacitive sensor noise; (ii) the amplitude fluctuations of the reference voltage sources V_p (DC) and V_d (sine wave at 10^5 Hz); these sources have already been developed for GRADIO; they present fluctuations of $\delta V_p = 12 \times 10^{-8} \times \frac{1}{10} V_p \sqrt{(1 + 7/f)}$ and $\delta V_{d_{rms}} = 2 \times 10^{-6} \times \frac{1}{5} V_{d_{rms}} \sqrt{(1 + 0.3/f)}$ these fluctuations generate electrostatic force variations through configuration asymmetry; an accuracy of 1 μm has been considered for the radius of the cylinders and the off-centring of the test mass along the sensitive axis is assumed to be < 10 μm with respect to the cage; (iii) the thermodynamic noise resulting from the test-mass motion damping induced mainly by the wire fixed to the test mass; a wire stiffness of 10^{-6} N m^{-1} and a quality factor of 10^5 have been considered; (iv) the noise of the measurement pick-off amplifier. As shown in figure 7 for the Pt test-mass accelerometer, the evaluated resolution is better than 10^{-14} m s^{-2} $Hz^{-1/2}$ for frequencies $< 2 \times 10^{-3}$ Hz.

Other accelerometer noise sources have been considered for the evaluation of SAGE. The residual pressure inside the accelerometer cage could generate radiometric effects, acoustic effects or motion dampings but the levels of the induced accelerations remain negligible because the expected pressure is lower than 10^{-6} Pa at 4 K. The test masses also benefit from a superconducting shield to avoid disturbances induced by the variations of satellite

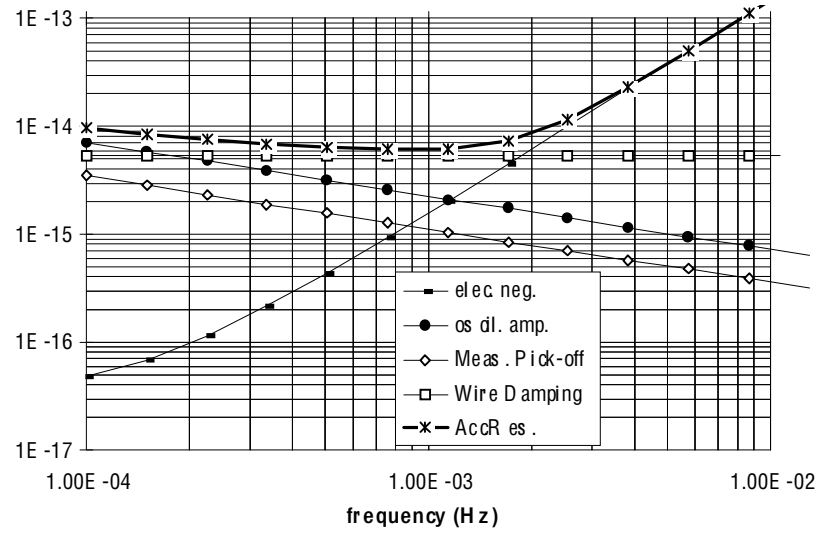

Figure 7. Accelerometer resolution versus the frequency.

magnetic moments or Lorentz forces that may act on any test-mass charge-crossing magnetic field lines, as in the case of the inertial sensor of the LISA mission, for instance [11]. At low frequencies, the accelerometer resolution is mainly driven by the dissipation, as is also concluded in [12].

Besides the sensor resolution, the stability of the scale factors and of the axis alignments must be sufficient to preserve the matchings between both accelerometers (of one SAGE). The thermal stability inside the helium cryostat, given the low coefficient of thermal expansion of the silica (5×10^{-7} °C^{-1}) used for the accelerometer parts leads to a high stability of the geometry on which the electrostatic configuration around the test mass depends. Also the alignment stability depends directly on the proof-mass attitude control accuracy but ground tests in ONERA of the GRADIO space accelerometers devoted to the ARISTOTELES mission have shown that an accuracy of much better than 10^{-7} rad can be reached with electrostatic accelerometers [13]. The scale factor stability will mainly depend on the V_p reference voltage stability which can be better than 10^{-6}; this is sufficient because the satellite drag compensation system will limit the instrument full scale range.

5. Conclusions

From experience acquired with the development of the space accelerometers GRADIO and ASTRE, using electrostatic suspension of a test mass, the configuration of the SAGE differential accelerometer has been defined specifically for a test in space of the equivalence principle to an accuracy of 10^{-17}.

The mechanical design of the sensor head is based on two concentric cylindrical test masses that are suspended electrostatically, the six degrees of freedom of each test mass being controlled independently. SAGE is then composed of two accelerometers that can be integrated and tested separately. Each accelerometer cage is made of fused silica with a set of electrodes defined by coatings and optimized to obtain the best resolution along the axial direction while the resolution in the radial directions is sufficient for the drag compensation system of the satellite. The geometry of the parts has been defined and the

electrostatic configuration has been analysed in order to determine the sensitivity of the capacitive sensing and of the electrostatic actuators.

The room-temperature electronics for each accelerometer will include six servo-loops with six capacitive sensors exhibiting position resolutions that do not limit the accelerometer resolution in the low-frequency bandwidth of the EP test.

A very thin gold wire of 5 μm diameter is presently proposed to manage the test-mass electrical potential, in this way suppressing the disturbances induced by the charges acquired by the mass in orbit subjected to the proton flux of the South Atlantic Anomaly, in particular [14]. This solution has already been selected and implemented in the GRADIO and ASTRE accelerometers. Because this wire could be a limitation to the performance of the SAGE accelerometer, experimental investigations have been undertaken to measure directly the stiffness and the damping added by the wire to the suspended test mass. It has already been demonstrated that the wire has a stiffness lower than 10^{-4} N m^{-1}. But, to demonstrate the specifications, a special torsion balance is being realized. The arm of this balance will be suspended electrostatically with a very weak stiffness in rotation and the gold wire will be implemented in such a way as to generate a torque about the vertical axis. The attitude of the arm will be measured with capacitive sensing and a resolution of 10^{-13} Nm Hz$^{-1/2}$ appears to be achievable even at frequencies lower than 0.1 Hz, when considering the demonstrated performances of the proof-mass attitude control of the GRADIO accelerometer.

The operation of SAGE at room temperature will facilitate the ground tests and calibrations that can be performed by adding to the flight electronics a booster electronics with 1000 V amplifiers necessary to sustain normal gravity. As has been done for the ASTRE accelerometer, the sensitive axis configuration is preserved during these tests that can then be very representative of the in-orbit operation. The operation of such electrostatic accelerometers allows easy tests in microgravity conditions in a drop tower. Tests in free-fall have been performed with ASTRE in the ZARM facility (Bremen, Germany) and have shown that the 4.7 s of fall is sufficient to obtain the test-mass electrostatic suspension and the nominal accelerometer operation. The very low power consumption in the SAGE sensor-head allows operation at liquid helium temperature for the ultimate resolution that should be limited at the low frequencies of the EP test by the quality factor of the test-mass axial motion.

From the present definition of the sensor head, the production of the first laboratory model is expected to start in 1996, bearing in mind that the development of such a space accelerometer needs several years and that the launch of a satellite for the test in space of the equivalence principle is expected at the beginning of the next century.

Acknowledgments

The analysis of the test in space of the equivalence principle and the development of the SAGE accelerometer is carried out at ONERA under contract with CNES and with the support of internal funding.

References

[1] Everitt C W F *et al* 1995 Satellite test of the equivalence principle *'Quick STEP' phase A study report* JPL D-12453

[2] Blaser J P *et al* 1993 STEP: satellite test of the equivalence principle *Report on the phase A study* ESA SCI (93)

[3] Bonneville R 1995 GeoSTEP geodesy experiment in space and satellite test of the equivalence principle CNES DDPI/DPS

[4] Worden P Jr, Everitt C W F and Bye M 1990 *Satellite Test of the Equivalence Principle: Science Requirements Document* Stanford University

[5] Damour T and Blaser J P 1995 *Optimising the Choice of the Materials in Equivalence Principle Experiments* XXX Rencontres de Moriond

[6] Touboul P, Rodrigues M and Willemenot E 1995 *GeoSTEP: Mission Analysis and Requirements* RTS 18/3815 PY, ONERA Châtillon

[7] Lockerbie N A, Veryaskin A V and Su X 1993 Differential gravitational coupling between cylindrically symmetric concentric test-masses and arbitrary gravitational source *Class. Quantum Grav.* **10** 2419–30

[8] Ravex A and Viargues F 1996 A supercritical superfluid helium cryostat for geostep: preliminary study *Class. Quantum Grav.* **13** A171–7

[9] Touboul P *et al* 1994 Continuation of the GRADIO accelerometer development *ONERA final report* 62/6114 PY, ESTEC Noordwijk

[10] Nati M, Bernard A, Foulon B and Touboul P 1994 ASTRE a highly performant accelerometer for the low frequency range of the microgravity environment *24th Int. Conf. on Environment Systems (Friedrichshafen)*

[11] Rodrigues M, Touboul P and Le Clerc G M 1996 The inertial reference sensor CAESAR for the laser interferometer space antenna mission *Class. Quantum Grav.* **13** A259–70

[12] Maraner A, Vitale S and Zendri J P 1996 A performance comparison between superconductivity and electrostatic gravity gradiometers *Class. Quantum Grav.* **13** A129–33

[13] Touboul P, Foulon B and Bernard A 1994 *Electrostatic Servocontrolled Accelerometers for Future Space Missions* Tire a part N 1994-144, ONERA Châtillon

[14] Juillerat R, Phillipon J P, Barlier F and Villain J P 1977 Electrisation en orbite de la masse d'épreuve d'un accélérometre a très haute sensibilité *Extrait des comptes rendus de l'Académie des Sciences* t.248B p 275–8